

Discovery of a *Plasmodium falciparum* Glucose-6-phosphate Dehydrogenase 6-phosphogluconolactonase Inhibitor (*R,Z*)-*N*-((1-Ethylpyrrolidin-2-yl)methyl)-2-(2-fluorobenzylidene)-3-oxo-3,4-dihydro-2*H*-benzo[*b*][1,4]thiazine-6-carboxamide (ML276) That Reduces Parasite Growth in Vitro

Janina Preuss,^{†,‡,§,⊥} Patrick Maloney,^{⊥,⊥} Satyamaheshwar Peddibhotla,^{⊥,⊥} Michael P. Hedrick,^{§,⊥} Paul Hershberger,^{⊥,⊥} Palak Gosalia,[§] Monika Milewski,[§] Yujie Linda Li,[§] Eliot Sugarman,[⊥] Becky Hood,[⊥] Eigo Suyama,[⊥] Kevin Nguyen,[⊥] Stefan Vasile,[⊥] Eduard Sergienko,[§] Arianna Mangravita-Novo,[⊥] Michael Vicchiarelli,[⊥] Danielle McAnally,[⊥] Layton H. Smith,[⊥] Gregory P. Roth,[⊥] Jena Diwan,[§] Thomas D.Y. Chung,[§] Esther Jortzik,[‡] Stefan Rahlfs,[‡] Katja Becker,^{*,‡} Anthony B. Pinkerton,^{*,§} and Lars Bode^{*,†}

[†]Department of Pediatrics, University of California, San Diego, La Jolla, California 92037, United States

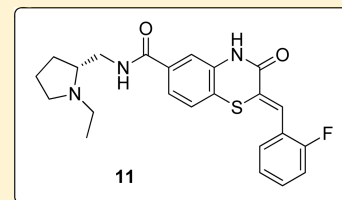
[‡]Biochemistry and Molecular Biology, Interdisciplinary Research Center, Justus Liebig University, Heinrich-Buff-Ring 26-32, 35392 Giessen, Germany

[§]Conrad Prebys Center for Chemical Genomics, Sanford–Burnham Medical Research Institute, La Jolla, California 92037, United States

[⊥]Conrad Prebys Center for Chemical Genomics, Sanford–Burnham Medical Research Institute, Orlando, Florida 32827, United States

Supporting Information

ABSTRACT: A high-throughput screen of the NIH's MLSMR collection of ~340000 compounds was undertaken to identify compounds that inhibit *Plasmodium falciparum* glucose-6-phosphate dehydrogenase (*Pf*G6PD). *Pf*G6PD is important for proliferating and propagating *P. falciparum* and differs structurally and mechanistically from the human orthologue. The reaction catalyzed by glucose-6-phosphate dehydrogenase (G6PD) is the first, rate-limiting step in the pentose phosphate pathway (PPP), a key metabolic pathway sustaining anabolic needs in reductive equivalents and synthetic materials in fast-growing cells. In *P. falciparum*, the bifunctional enzyme glucose-6-phosphate dehydrogenase-6-phosphogluconolactonase (*Pf*GluPho) catalyzes the first two steps of the PPP. Because *P. falciparum* and infected host red blood cells rely on accelerated glucose flux, they depend on the G6PD activity of *Pf*GluPho. The lead compound identified from this effort, (*R,Z*)-*N*-((1-ethylpyrrolidin-2-yl)methyl)-2-(2-fluorobenzylidene)-3-oxo-3,4-dihydro-2*H*-benzo[*b*][1,4]thiazine-6-carboxamide, **11** (ML276), is a submicromolar inhibitor of *Pf*G6PD (IC₅₀ = 889 nM). It is completely selective for the enzyme's human isoform, displays micromolar potency (IC₅₀ = 2.6 μM) against *P. falciparum* in culture, and has good drug-like properties, including high solubility and moderate microsomal stability. Studies testing the potential advantage of inhibiting *Pf*G6PD in vivo are in progress.



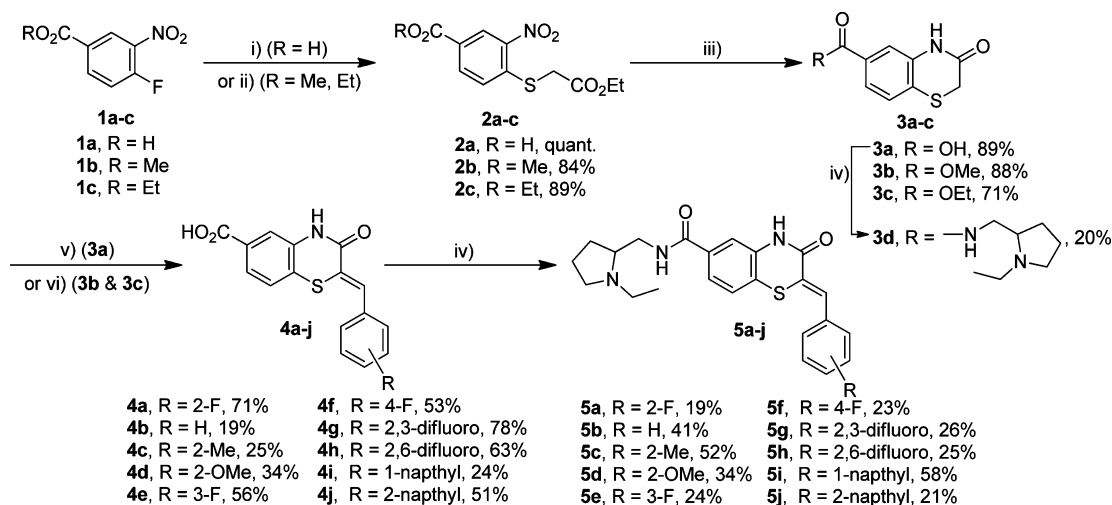
INTRODUCTION

In 2010, around 1.2 million people died from malaria infections.¹ Severe forms of the disease are mainly caused by *Plasmodium* parasites of the species *falciparum*, which are transmitted to the human host by female *Anopheles* mosquitoes.² *P. falciparum* parasites have infected humans for thousands to millions of years,^{3,4} and yet malaria eradication has not been possible due to the parasites' ability to develop resistance to most antimalarial drugs.⁵ To date, no vaccine against malaria is available,⁶ and infections are treated with drugs commonly targeting the blood stage of the parasite.⁷ The most common clinically used antimalarial drugs belong to seven

classes, namely 4-aminoquinolines such as chloroquine and amodiaquine, arylaminoalcohols such as quinine and mefloquine, 8-aminoquinolines such as primaquine, artemisinins such as artemether and artesunate as well as synthetic peroxides such as tri- and tetraoxanes,⁸ antifolates such as sulfadoxine and pyrimethamine, inhibitors of the respiratory chain such as atovaquone, and antibiotics.^{9,10} The occurrence of drug-resistant *P. falciparum* strains^{11–13} as well as side effects from drug administration^{14,15} resulted in the current WHO

Received: June 13, 2012

Published: July 19, 2012

Scheme 1. Synthesis of 5a and Analogues^a

^aConditions: (i) ethyl thioglycolate, NaOAc, H₂O, 90 °C; (ii) ethyl thioglycolate, triethylamine, MeCN, 85 °C; (iii) Fe, HOAc, 80 °C; (iv) 2-aminomethyl-1-ethylpyrrolidine, EDCI-HCl, HOBt, Et₃N, CH₂Cl₂, 23 °C; (v) aldehyde, Ac₂O, Et₃N, reflux; (vi) aldehyde, Ac₂O, Et₃N, reflux; LiOH, MeOH, H₂O, 23 °C.

recommendation to use artemisinin-based combination therapies to treat *P. falciparum* malaria.¹⁶ However, recent reports of artemisinin resistances^{17–19} again create an urgent need for new antimalarial drugs. On the basis of several findings, the enzyme glucose-6-phosphate dehydrogenase 6-phosphogluconolactonase of *P. falciparum* (*PfGluPho*) has emerged as an intriguing new target for antimalarial drug development.²⁰ Deficiency in human glucose-6-phosphate dehydrogenase (hG6PD), which affects around 330 million people worldwide,²¹ is associated with protection from severe malaria infections.^{22–24} It is suggested that both hG6PD and *PfGluPho* play an important role in *Plasmodium* development and survival.^{20,22,25} *PfGluPho* is the key enzyme of the parasitic pentose phosphate pathway (PPP), which is supposed to be the major NADPH source (reviewed by Preuss et al.²⁶) for these parasites highly sensitive to oxidative stress.²⁷ A previous study showed that *P. falciparum*-infected red blood cells (IRBC) present an increased PPP activity compared to noninfected ones, 80% of which is caused by *Plasmodium*'s PPP.²⁵ Moreover, silencing of *PfGluPho* with RNA interference (RNAi) stopped parasite development at the trophozoite stage.²⁸ Although Baum et al. reported in 2009 that *P. falciparum* lacks an RNAi machinery,²⁹ Lopez-Barragan et al. recently reported that antisense RNA may be an important factor in *P. falciparum*'s regulation of gene expression,³⁰ strengthening the results of the previous RNAi-based study. Additionally, *PfGluPho* presents considerable structural differences compared to hG6PD, potentially allowing selective targeting.^{31,32}

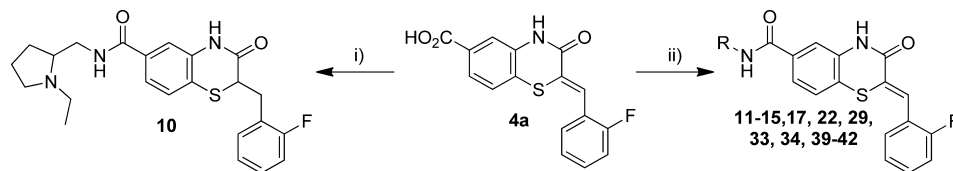
Herein we describe the high-throughput screening (HTS) of 348911 compounds in the NIH's Molecular Libraries Small Molecule Repository (MLSMR) collection (<http://mli.nih.gov/mli/compound-repository/mlsmr-compounds>) against *PfGluPho* and a subsequent structure–activity relationship (SAR) study of a class of benzothiazinone hits obtained from the screen. Optimization of the screening hits resulted in the discovery of (*R,Z*)-*N*-((1-ethylpyrrolidin-2-yl)methyl)-2-(2-fluorobenzylidene)-3-oxo-3,4-dihydro-2*H*-benzo[*b*][1,4]thiazine-6-carboxamide, **11** (ML276),³³ which inhibited *PfGluPho* selectively over hG6PD and inhibited *P. falciparum* growth in vitro with an IC₅₀ in the low micromolar range. Compound **11**

represents the first reported selective *PfGluPho* inhibitor and therefore could provide a basis for future drug design of new antimalarial therapeutics.

RESULTS AND DISCUSSION

High-Throughput Screening. In a primary screening approach, the MLSMR compound library (~350000 compounds) was screened at a concentration of 20 μM against *PfGluPho*. The screening campaign resulted in the identification of 2709 compounds that inhibited *PfGluPho* activity ≥59%, corresponding to a hit rate of 0.8%. Of these, 2429 were available from the MLSMR collection and were retested in triplicate at a concentration of 20 μM, resulting in 817 compounds inhibiting *PfGluPho* ≥50%, about 34% of the samples. To exclude samples that interfere with the coupled resazurin/diaphorase system used in our study,³⁴ active compounds were run against a diaphorase inhibition assay at a concentration of 20 μM. Of the compounds tested, 230 inhibited the diaphorase reaction and thus were discarded as artifacts. The remaining 587 active compounds were further tested in dose response in the *PfGluPho* assay and an hG6PD counter-screen. As a result, 488 compounds presented IC₅₀ values ≤20 μM vs *PfGluPho*, and only 39 of the compounds were active against hG6PD. For final confirmation, the compounds were tested in an orthogonal assay that did not rely on the resazurin and diaphorase coupled system. On the basis of the initial slope of the reaction, around 50% of the compounds were confirmed to inhibit *PfGluPho* with an IC₅₀ ≤ 80 μM. Several series of compounds were identified, of which a group of benzothiazinones was most promising based on their potency and selectivity. Detailed information is available in the PubChem database (AIDs 504690, 504753, 504863, 504862, 504765, 504792, 540252, 540269).

Synthesis. The synthesis of the benzothiazinone-derived compounds described herein was accomplished in 4–5 steps as outlined in Scheme 1.³⁵ Starting from 4-fluoro-3-nitrobenzoic acid or the esters (**1a–1c**), nucleophilic substitution of the fluorine substituent with ethyl thioglycolate under basic conditions provided thioethers (**2a–2c**). Reductive cyclization mediated by iron in acetic acid provided benzothiazinones

Scheme 2. Synthesis of Compounds 10–15, 17, 22, 29, 33, 34, and 39–42 including 11^a.

^aConditions: (i) CoCl_2 , NaBH_4 , THF, 23°C , 53%, 2-aminomethyl-1-ethylpyrrolidine, EDCI·HCl, HOBT, Et_3N , CH_2Cl_2 , 23°C , 41%; (ii) RNH_2 , EDCI·HCl, HOBT, Et_3N , CH_2Cl_2 , 23°C , 13–61%.

(3a–3c). 1-Ethyl-3-(3-dimethylaminopropyl) carbodiimide (EDCI)-mediated coupling of 3a with 2-aminomethyl-1-ethylpyrrolidine afforded amide 3d. The first point of diversity was introduced by condensation of benzothiazinones (3a–3c) with a range of aromatic aldehydes resulting in intermediates (4a–4j). Coupling of intermediates (4a–4j) with 2-aminomethyl-1-ethylpyrrolidine resulted in the corresponding amides 5a–5j (Scheme 1). The styryl moiety in the intermediate 4a was reduced with sodium borohydride in the presence of cobalt chloride, and the resulting acid was converted to amide 10 (Scheme 2). A second point of diversity resulted from amide synthesis starting from 4a using diverse amines to provide the amides 10–15, 17, 22, 29, 33, 34, and 39–42 (Scheme 2). All final compounds were obtained in moderate yields and high purity needed to support SAR studies.

Structure–Activity Relationships (SAR). Three main assays were utilized to direct the SAR efforts. The primary SAR-driving assay was the dose response, resazurin/diaphorase-coupled *Pf*GluPho assay, with the hG6PD assay serving as the counter-screen to ascertain specificity. None of the compounds from this series showed any activity in the hG6PD counter-screen ($>80\ \mu\text{M}$) and thus were considered specific for the *P. falciparum* enzyme. The orthogonal *Pf*GluPho assay, which relied on the direct detection of NADPH, was used to further confirm activity in the absence of the coupled resazurin/diaphorase system. Of the 156 substituted benzothiazinones tested in the high-throughput screen, only five were confirmed active by dose response. All were inactive ($\text{IC}_{50} > 80\ \mu\text{M}$) against hG6PD. These structures are represented in Table 1. The structural features of these active benzothiazinones that separate them from those that were either inactive or failed confirmation in dose response include: (1) the amide side chain contains a basic alkylamine, (2) the nitrogen in the benzothiazinone ring is not alkylated, and (3) the sulfur exists as a sulfide (Figure 1).

From this preliminary SAR, we focused on further optimization of the scaffold. Specifically, we examined a wide range of amide substitutions as well as substitution around the pendant aryl ring. The general SAR strategy is depicted in Figure 2.

Exploration of the styryl SAR was initiated by maintaining the preferred 1-ethyl-2-amino-methylpyrrolidine moiety from the HTS data and is summarized in Table 2. The primary hit 5a, identified during the HTS and subsequent hit confirmation, was resynthesized as described in Scheme 1. It was equipotent to the purchased compound (entry 5a, Tables 1 and 2). ^1H NMR data of the purchased sample and the synthesized sample of 5a were identical. The *Z*-geometry around the styryl portion was assigned based on comparison to previously reported NMR data.³⁶

A variety of substituted styryl analogues were synthesized; however, the potency range was only affected by 7-fold. The 2-

Table 1. Structures of Active Benzothiazinone Hits from HTS

Entry	Structure	<i>Pf</i> G6PD IC_{50} (μM)
5a		1.75
6		2.56
7		4.42
8		9.30
9		17.9

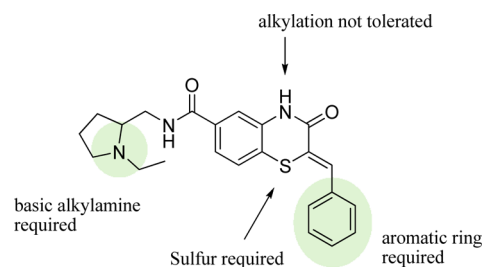


Figure 1. Structural requirements for activity.

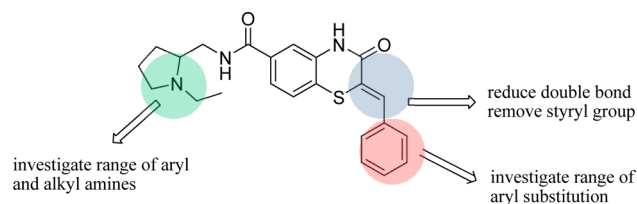
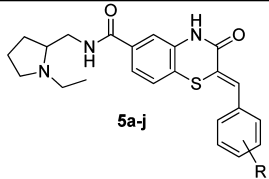


Figure 2. General SAR strategy.

Table 2. SAR of Benzothiazinones^a Inhibiting *Plasmodium falciparum* Glucose-6-phosphate Dehydrogenase

		Potency (μM) Ave. \pm S.E.M. ($n = 4$)	
Compound	R	PfG6PD Primary Assay	PfG6PD NADPH Kinetic
5a	2-F	1.73 \pm 0.08	1.37
5b	H	8.23 \pm 2.11	19.7
6^b	2-Cl	2.56 \pm 0.19	3.3
5c	2-Me	5.93 \pm 1.59	5.01
5d	2-OMe	9.79 \pm 1.13	11.3
5e	3-F	2.35 \pm 0.29	4.13
5f	4-F	1.41 \pm 0.14	2.06
7^b	4-Me	4.42 \pm 0.71	11.6
5g	2,3-difluoro	5.72 \pm 1.28	3.89
5h	2,6-difluoro	1.65 \pm 0.08	2.61
5i	1-naphthyl	4.28 \pm 0.87	4.2
5j	2-naphthyl	2.39 \pm 0.28	2.88

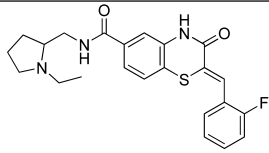
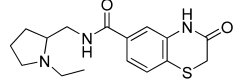
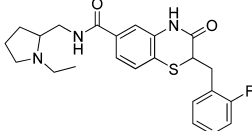
^aAll compounds represented in this table exhibited an $\text{IC}_{50} > 80 \mu\text{M}$ against human G6PD. ^bScreen hit.

fluoro substituent is important for activity, as the analogue without any aryl substituent was ~ 4 -fold less active (entry **5a** vs **5b**, Table 2). Interestingly, neither the position nor the electronics of the substituent dramatically affected the observed potency. For example, analogues containing the 2-, 3-, or 4-fluoro substitution (entries **5a**, **5e**, and **5f**, Table 2) were essentially equipotent. Replacement of the 2-fluoro substituent with 2-chloro did not significantly affect the potency, but replacement with electron-rich 2-methyl or 2-methoxy groups decreased potency by 3-fold and 5-fold, respectively (entries **5a**, **6**, **5c**, and **5d**, Table 2). Fused ring systems such as 1-naphthyl and 2-naphthyl (entries **5i** and **5j**, Table 2) also slightly lowered potency. The unsubstituted phenyl and the 2-methoxy analogues (entries **5b** and **5d**, Table 2) were the least preferred of the synthesized analogues.

While the SAR around the styryl moiety may appear to minimally affect potency, its presence was required for activity. When the styryl group was replaced with phenethyl or removed entirely, a complete loss of activity resulted (**5a** vs **3d** and **10**, Table 3).

The SAR of the alkylamino side chain proved to be much more stringent than the styryl region, with a strong preference for 2-aminomethyl pyrrolidines. Potency was maintained within 5-fold whether the nitrogen of the pyrrolidine ring was substituted with ethyl, propyl, or was unsubstituted (entries **5a**, **13** and **15**, Table 4). The *t*-butoxycarbonyl derivative proved inactive, consistent with observations from the HTS (entry **14**, Table 4). Less constrained examples such as dimethylaminoethyl, diethylaminoethyl, and dipropylaminoethyl demonstrated sharp decreases in potency (entries **16–27**, Table 5). Attachment of pyrrolidine through nitrogen via an aminoethyl linker led to a 5-fold loss of potency, which became

Table 3. Necessity of Styryl Moiety in SAR

Entry	Structure	PfG6PD IC_{50} (μM)
5a		1.73
3d		>80
10		>80

more pronounced as the ring was expanded (entries **8**, **9**, **28–39**, Table 6). Examples of constrained tertiary or aromatic amides proved substantially less active (entries **40–42**, Table 6). All compounds represented in Tables 4, 5, and 6 exhibited an $\text{IC}_{50} > 80 \mu\text{M}$ against hG6PD.

Stereochemical evaluation of the 2-aminomethyl pyrrolidines led us to synthesize each enantiomer of **5a** from the corresponding commercially available chiral amines. An 8-fold preference for the *R*-enantiomer versus the *S*-enantiomer was discovered (entries **11** and **12**, Table 4). Compound **11**, (*R,Z*)-*N*-((1-ethylpyrrolidin-2-yl)methyl)-2-(2-fluorobenzylidene)-3-oxo-3,4-dihydro-2*H*-benzo[*b*][1,4]thiazine-6-carboxamide, was the most potent compound identified and was therefore declared a probe. Compound **11** was selective for *PfGluPho* over hG6PD (Figure 3).

In Vitro ADME/T Profiling and Chemical Stability.

Compound **11** was evaluated in a detailed in vitro pharmacology screen (absorption, distribution, metabolism, excretion, toxicity (ADME/T)) as shown in Table 7. Compound **11** is highly soluble, especially at lower pH, which is likely due to the presence and protonation of the alkylamino moiety.

Consistent with its solubility data, **11** exhibits high permeability with increased pH of the donor compartment in a standard parallel artificial membrane permeability assay (PAMPA). When incubated with an artificial membrane that models the blood–brain barrier (BBB), **11** was highly permeable. Compound **11** had good stability in plasma, thus increasing its exposure to blood-borne parasites such as *P. falciparum*, and it was highly plasma protein bound, which may contribute to its high plasma stability. Lastly, **11** shows moderate stability in human and modest stability in mouse liver homogenates and no toxicity ($>50 \mu\text{M}$) toward Fa2N-4 immortalized human hepatocytes.

Compound **11** contains an α,β -unsaturated amide and is a potential Michael acceptor. To investigate this potential chemical liability, **11** ($10 \mu\text{M}$, 1% DMSO) was incubated with 5 equiv of glutathione (GSH) in PBS buffer (pH 7.4) at 23°C . Loss of compound was monitored at different times over 18 h using RP-LCMS (Figure 4). Ethacrynic acid, a diuretic containing an α,β -unsaturated ketone, was used as a positive control because it has been previously reported to form a GSH-adduct.³⁷ Loss of ethacrynic acid was observed as early as 30 min and was $\sim 97\%$ depleted in 24 h, whereas **11** remained

Table 4. SAR of Benzothiazinones Inhibiting *Plasmodium falciparum* Glucose-6-phosphate Dehydrogenase

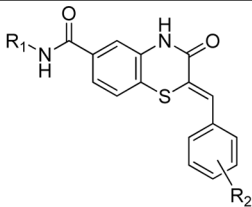
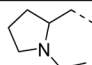
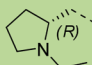
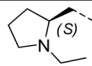
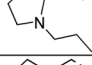
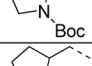

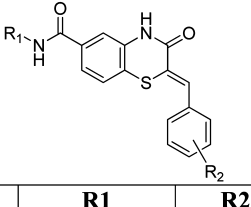
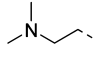
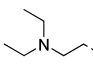
				Potency (μM) Ave. \pm S.E.M.	
Entry	R1	R2	Yield %	<i>Pf</i> G6PD Primary Assay	<i>Pf</i> G6PD NADPH Kinetic
5a racemic		2-F	19	1.7 ± 0.1	1.4
11 <i>R</i> -enantiomer ML276		2-F	32	0.9 ± 0.0	1.9
12 <i>S</i> -enantiomer		2-F	28	6.6 ± 0.2	4.7
13		2-F	48	3.1 ± 0.4	4.0
14		2-F	61	>80.0	24.4
15		2-F	79	5.9 ± 0.6	5.0

Table 5. SAR of Benzothiazinones Inhibiting *Plasmodium falciparum* Glucose-6-phosphate Dehydrogenase

				Potency (μM) Ave. \pm S.E.M.	
Entry	R1	R2	Yield % ^a	<i>Pf</i> G6PD Primary Assay	<i>Pf</i> G6PD NADPH Kinetic
16		2-F	P	16.7 ± 0.8	11.2
17		2-F	13	17.5 ± 8.5	38.4
18		3-Cl	P	60.0 ± 8.5	43.6
19		4-OMe	P	>80.0	>80.0
20		H	P	8.8 ± 1.6	18.4
21		2-F	P	7.4 ± 0.7	9.4
22		2-F	28	6.9 ± 0.3	4.8
23		2-Cl	P	16.2 ± 2.1	44.9
24		3-Me	P	14.5 ± 3.8	18.8
25		3,4-(OMe) ₂	P	60.0 ± 10.0	24.5
26		H	P	>80.0	27.2
27		4-Me	P	>80.0	45.9

^aP: commercially purchased compounds.

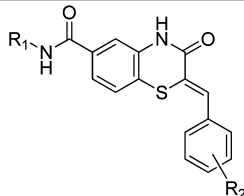
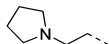
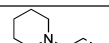
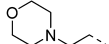
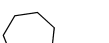
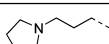
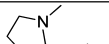
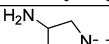
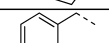
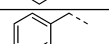
intact for the duration of the study, indicating a lack of reactivity with nucleophiles (Figure 4). Thus, **11** represents a potential lead compound for the development of an in vivo probe.

Activity against *P. falciparum* in Culture. Compound **11** was included in *P. falciparum* growth assays to assess its effects on blood stage parasites in vitro. After incubation for 72 h, **11** gave IC₅₀ values of $2.3 \pm 0.2 \mu\text{M}$ for the chloroquine sensitive

3D7 strain and 3.7 ± 0.9 for the chloroquine resistant Dd2 strain (Figure 5).

Mechanism of Inhibition (MOI) Studies. The most likely type of inhibition was determined by titrating compound and substrate/cosubstrate at the same time. G6P and **11** titration revealed increasing K_m values and an $\alpha > 6.6$ with increasing compound concentration, suggesting that **11** inhibits *Pf*GluPho activity by competing with the substrate (Figure 6B). Increasing

Table 6. SAR of Benzothiazinones Inhibiting *Plasmodium falciparum* Glucose-6-phosphate Dehydrogenase

				Potency (μM) Ave. \pm S.E.M.	
Entry	R1	R2	Yield % ^a	<i>Pf</i> G6PD Primary Assay	<i>Pf</i> G6PD NADPH Kinetic
28		2-F	P	9.5 \pm 3.6	11.0
29		2-F	18	16.2 \pm 2.1	25.2
30		4-OMe	P	49.7 \pm 13.7	>80.0
31		2-Cl	P	11.1 \pm 1.3	>80.0
32		3-Me	P	11.8 \pm 0.4	8.8
33		2-F	6	21.6 \pm 3.4	24.0
34		2-F	15	>80.0	>80.0
35		2-F	P	46.6 \pm 10.0	11.0
36		2-Cl	P	40.9 \pm 12.5	>80.0
37		3-OMe	P	>80.0	58.5
38		4-OMe	P	>80.0	>80.0
8 ^b		H	P	9.3	22.3
9 ^b		3-Cl	P	17.9	34.2
39		2-F	27	22.7 \pm 2.1	45.2
40		2-F	36	45.0 \pm 5.3	35.0
41		2-F	36	>80.0	>80.0
42		2-F	46	>80.0	67.8

^aP: commercially purchased compounds. ^bScreen hit.

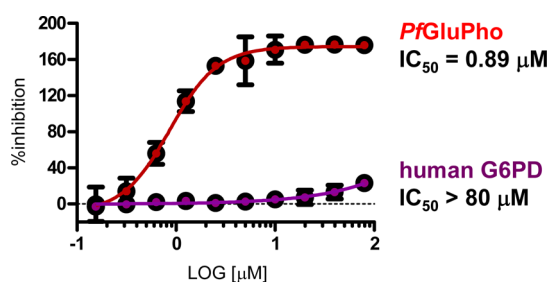


Figure 3. Dose–response curve for **11** in the *Plasmodium* and human G6PD assays, indicating full selectivity for *Pf*GluPho.

K_m and decreasing V_{max} values, and α between 1.4 and 4.7, were found when compound and cosubstrate were titrated, indicating mixed-type inhibition of **11** vs NADP⁺ (Figure 6A).

CONCLUSIONS

A series of benzothiazinones derived from an HTS of the NIH's MLSMR collection that are potent, fully selective inhibitors of *Pf*GluPho has been reported. The most potent compound in this series, **11**, has antimalarial activity against both chloroquine-sensitive and chloroquine-resistant strains. Compound **11** has reasonable in vitro ADME/T properties,

Table 7. Summary of in Vitro ADME/T Properties of *P. falciparum* G6PD Inhibitor Probe **11**

aqueous solubility in pION's buffer ($\mu\text{g/mL}$) [μM] ^a pH 5.0/6.2/7.4	>126/>126/29.4 [>296/>296/69]
aqueous solubility in 1 \times PBS, pH 7.4 ($\mu\text{g/mL}$) [μM] ^a	71.0 [166]
PAMPA permeability, P_e ($\times 10^{-6}$ cm/s) donor pH, 5.0/6.2/7.4; acceptor pH, 7.4	29/737/806
BBB–PAMPA permeability, P_e ($\times 10^{-6}$ cm/s) donor pH, 7.4; acceptor pH, 7.4	233
plasma protein binding (% bound)	human 1 μM /10 μM 98.39/97.98 mouse 1 μM /10 μM 98.95/98.34
plasma stability (% remaining at 3 h) human/mouse	90.98/80.84
hepatic microsomal stability (% remaining at 1 h) human/mouse	60.53/37.57
toxicity toward Fa2N-4 immortalized human hepatocytes LC_{50} (μM)	>50

^aSolubility also expressed in molar units (μM) as indicated in italicized [bracketed values], in addition to more traditional $\mu\text{g/mL}$ units.

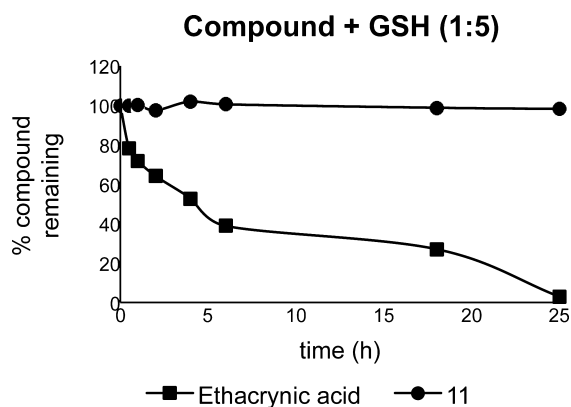


Figure 4. Investigation of chemical reactivity/stability of **11** via GSH adduct formation.

including excellent solubility, no toxicity, good permeability and plasma stability, and moderate microsomal stability. Further work in this series is in progress to optimize the potency and ADME/T properties, which may lead to validation in *in vivo* models.

EXPERIMENTAL SECTION

HTS/Biology. Materials. G6P, resazurin, diaphorase, Tween20, $MgCl_2$, and BSA were obtained from Sigma, St. Louis, MO. $NADP^+$ was purchased from Amresco, Solon, OH, and 1536 well-plates from Aurora, Poway, CA.

Compound Library. The Sanford–Burnham Center for Chemical Genomics' copy of the NIH Molecular Libraries Small Molecule Repository (MLSMR) consisted of 348911 compounds when the screen was run, which were present in 1536-well plates at a concentration of 2 mM (in DMSO). The library was stored at $-80^\circ C$ until first use, after which it was kept at room temperature under desiccating conditions for a period not greater than six months.

HTS. Primary Screen. The previously developed HTS assay for *PfGluPho*³⁴ was used in a 384-well plate format. This assay was slightly modified for use in 1536-well plates and performed in the following way. A volume of 60 nL of the compounds (final 20 μM , 1% DMSO) was transferred to columns 5–48 of 1536-well plates using the Echo Liquid Handler (LabCyte). Then 60 nL of DMSO were transferred to columns 1–4, which served as positive and negative controls. A volume of 3 μL of enzyme mix (50 mM Tris (pH 7.5), 0.005% Tween 20, 1 mg/mL BSA, 0.1 $\mu g/mL$ *PfGluPho*) was added to all wells using the Kalypsys (Kalypsys Systems). To start the reaction, 3 μL of substrate mix (50 mM Tris (pH 7.5), 40 μM G6P, 0.005% Tween 20, 1 mg/mL BSA, 6 μM $NADP^+$, 6.6 mM $MgCl_2$, 2 U/mL diaphorase, 0.05 mM resazurin) were added to columns 3–48 using the Kalypsys. Substrate mix without G6P was added to columns

1–2 for positive control. The plates were centrifuged at 1500 rpm for 1 min and incubated in the dark for 2 h. Fluorescence of resorufin was detected at excitation 530/emission 580 nm (ex530/em580) using a Viewlux (PerkinElmer) plate reader. Data was analyzed with CBIS (Chemical and Biological Information Systems, www.cheminnovation.com), and compounds inhibiting *PfGluPho* for at least 59% were retested as described before. Retested compounds inhibiting *PfGluPho* activity $\geq 50\%$ were further investigated.

Diaphorase Counter-Screen. First, 12 nL of 10 mM compounds in DMSO were transferred into columns 5–48 of 1536-well plates using the Echo Liquid Handler. Next, 12 nL of DMSO were transferred to columns 1–4 for positive and negative controls. Subsequently, 3 μL of substrate mix (50 mM Tris (pH 7.5), 0.005% Tween20, 1 mg/mL BSA, 6.6 mM $MgCl_2$, 0.06 mM/0.02 mM $NADPH$, 0.05 mM resazurin) were added to columns 1–48 using the Multidrop Combi reagent dispenser (Thermo Scientific). To initiate the reaction, 3 μL of enzyme solution (50 mM Tris (pH 7.5), 0.005% Tween 20, 1 mg/mL BSA, 6.6 mM $MgCl_2$, 2 U/mL diaphorase) were added to columns 3–48 with the Multidrop Combi dispenser. For the negative control, 3 μL of the enzyme solution without diaphorase were added to columns 1–2. The plates were centrifuged at 1500 rpm for 1 min, incubated in the dark for 2 h, and read at ex530/em590 nm. Diaphorase inhibition was analyzed using CBIS, and compounds exhibiting at least 50% enzyme inhibition were assigned active status and thus not included in further experiments.

Hit Confirmation in Dose Response. Varying volumes of compounds in DMSO (starting final concentration of 20 μM) were transferred to columns 5–48 of 1536-well plates using the Echo Liquid Handler. DMSO was added to control and test compound wells to equilibrate DMSO concentrations across plate (final concentration of 1.0%). The remaining assay procedures for the *PfGluPho* assay were performed as described in the Primary Screen section. Compounds with an IC_{50} of ≤ 20 μM were further investigated.

hG6PD Counter-Screen. Using the Echo Liquid Handler, varying volumes of compounds (starting final concentration of 20 μM) were transferred to wells of columns 5–48 of 1536-well plates. DMSO was added to control and test compound wells to equilibrate DMSO concentrations across the plate (final concentration of 0.8%). Then 2.5 μL of enzyme solution (50 mM Tris (pH 7.5), 0.005% Tween 20, 1 mg/mL BSA, 0.05 $\mu g/mL$ hG6PD) were transferred to all wells. Following enzyme addition, 2.5 μL substrate solution (0.64 mM G6P, 50 mM Tris (pH 7.5), 0.005% Tween 20, 1 mg/mL BSA, 12 μM $NADP^+$, 6.6 mM $MgCl_2$, 2 U/mL diaphorase, 0.28 mM resazurin) were added to columns 3–48 and solution without G6P to columns 1–2 for positive control. After 1 min of centrifugation at 1500 rpm and 90 min incubation in the dark, fluorescence of resorufin was detected at ex530/em590 by using the Viewlux plate reader. IC_{50} values were calculated using CBIS.

Orthogonal Assay. Using the Echo Liquid Handler, varying volumes of compounds were transferred to wells of columns 5–48 of 1536-well plates. DMSO was added to control and test compound wells to equilibrate DMSO concentrations across the plate. Following

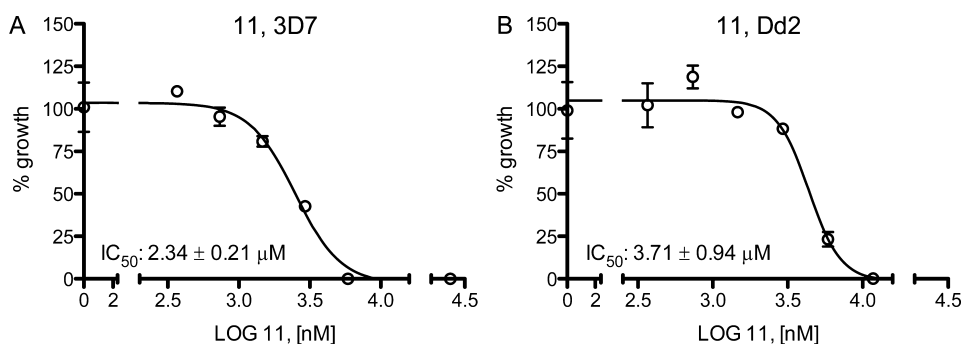


Figure 5. *P. falciparum* growth inhibition by **11** of chloroquine-sensitive (A) and chloroquine-resistant (B) strains. One representative data set out of two independent experiments is shown. Experiments were performed twice in triplicate, of which the average and standard deviation are given.

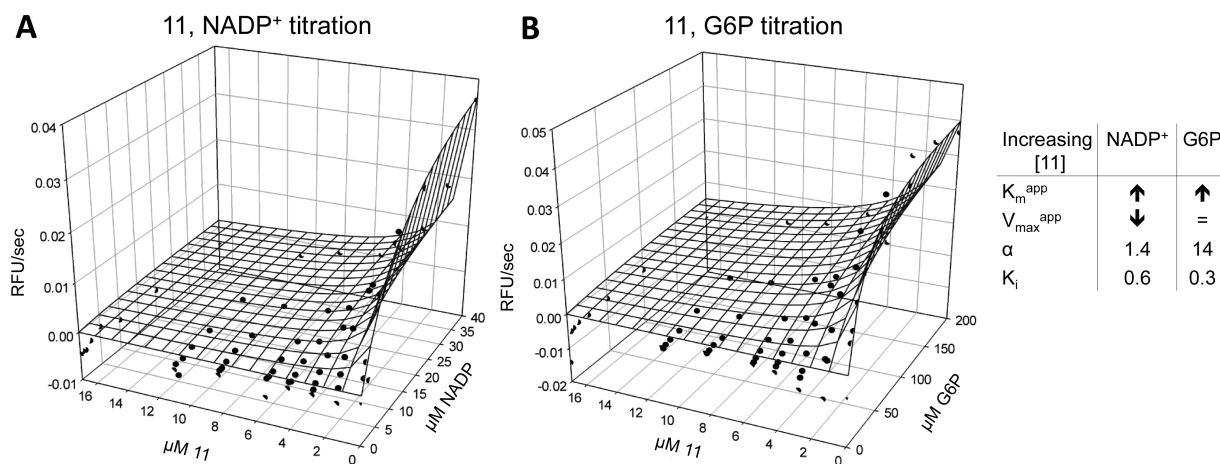


Figure 6. Mechanistic characterization of **11** vs NADP⁺ (A) and G6P (B) for PfGluPho. The signal (RFU/s) was plotted against the compound and NADP⁺ or G6P concentration. One representative data set from two independent experiments is shown. Data points are given as averages of duplicates.

compound and DMSO transfer, 2.5 μ L of enzyme solution (50 mM Tris (pH 7.5), 0.005% Tween 20, 1 mg/mL BSA, 0.4 μ g/mL PfGluPho) were added to all wells using a Multidrop Combi dispenser. Then 2.5 μ L of substrate solution (40 μ M G6P, 6 μ M NADP⁺, 50 mM Tris (pH 7.5), 0.005% Tween 20, 1 mg/mL BSA, 6.6 mM MgCl₂) were added to columns 5–48, and 2.5 μ L of solution without G6P were added to columns 1–4 for positive control. The plates were centrifuged and either incubated for 45 min to determine end points of the reaction or kinetically read at ex 340 nm/em 450 nm over 45 min. The reaction rate was calculated by dividing the relative fluorescence units (RFU) by time in minutes. CBIS was used to calculate IC₅₀ values, and compounds with IC₅₀ \leq 80 μ M were designated active.

Chemistry. All reactions involving air- and moisture-sensitive reagents and solvents were performed under a nitrogen atmosphere using standard chemical techniques. Anhydrous solvents were purchased and freshly used from Sigma-Aldrich or EMD Biosciences. All organic reagents were used as purchased. (*R*)-(1-ethylpyrrolidin-2-yl)methanamine (catalogue no. 35700010, CAS 22795–97–7) and (*S*)-(1-ethylpyrrolidin-2-yl)methanamine (catalogue no. 367750010, CAS 22795–99–9) were purchased from Acros Organics and used without further purification. Analytical thin-layer chromatography was performed on Partisil K6F silica gel 60 Å, 250 μ m. Microwave-assisted reactions were performed using a CEM Discover system. ¹H and ¹³C chemical shifts are reported in δ values in ppm in the corresponding solvent. All solvents used for chromatography on the synthetic materials were Fisher Scientific HPLC grade, and the water was Millipore Milli-Q PP filtered. All NMR spectra for the synthetic materials were recorded on a Bruker Avance II 400 or DRX-500 MHz instrument. High resolution mass spectrometry (HRMS) spectra were carried out on an Agilent 6224A Accurate-Mass time-of-flight (TOF) LC/MS system with electron spray ionization (ESI). LCMS analysis of synthetic materials was completed on a Waters Autopurification system, which consists of a 2767 sample manager, a 2545 binary gradient module, a system fluidics organizer, a 2489 UV/vis detector, and a 3100 mass detector, all controlled with MassLynx software. A Sunfire Analytical C18 5 μ m column (4.6 mm \times 50 mm) and stepwise gradient {10% [(MeCN + 0.1% TFA) in (water + 0.1% TFA)] to 98% [(MeCN + 0.1% TFA) in (water + 0.1% TFA)] for 9 min} was used for analytical LCMS of final compounds. The final compounds were purified by RP-HPLC on a SunFire preparative C18 column (5 μ m; 19 mm \times 50 mm) using a stepwise gradient {10% [(MeCN + 0.1% TFA) in (water + 0.1% TFA)] for 1 min; 30% for 1 min; 50% for 4 min; 70% for 1.5 min and 98% for 1.5 min}. All synthesized final compounds **5a–j** and **10–42** were determined to be \geq 95% pure by LC-MS. Compound identity was verified by ¹H NMR and HRMS, and additionally by ¹³C NMR for **11**. The MestReNova program was used to interpret NMR spectra.

General Procedure for the Synthesis of Compounds 5a–j and 10–42 as Illustrated by Synthesis of (*R,Z*)-N-((1-Ethylpyrrolidin-2-yl)methyl)-2-(2-fluorobenzylidene)-3-oxo-3,4-dihydro-2H-benzo[b][1,4]thiazine-6-carboxamide (11). 4-(2-Ethoxy-2-oxoethylthio)-3-nitrobenzoic Acid (**2a**). 4-Fluoro-3-nitrobenzoic acid (**1a**) (5.55 g, 30 mmol) and sodium acetate (2.71 g, 33 mmol) were combined in a round-bottom flask. Ethyl mercaptoacetate (3.62 mL, 33 mmol) and water (30 mL) were then added, and the mixture was heated under nitrogen atmosphere at 90 °C for 24 h. The reaction mixture was cooled to 23 °C and then placed in an ice bath for 10–20 min. The precipitate formed was collected by filtration, washed with water, and dried to afford **2a** as a tan solid (8.66 g, quant). ¹H NMR (500 MHz, CDCl₃) δ 9.02–8.91 (m, 1H), 8.34–8.20 (m, 1H), 7.64 (d, *J* = 8.6 Hz, 1H), 4.26 (q, *J* = 7.1 Hz, 2H), 3.84 (s, 2H), 1.31 (t, *J* = 7.1 Hz, 3H). LRMS (ESI-ve): calculated for C₁₁H₁₁NO₆S, [M – H] = 284.02; observed, [M – H] = 283.99.

3-Oxo-3,4-dihydro-2H-benzo[b][1,4]thiazine-6-carboxylic Acid (3a). **2a** (3.94 g, 13.8 mmol) and iron powder (3.08 g, 55 mmol) were suspended in glacial acetic acid (33 mL) in a round-bottom flask equipped with an air condenser under nitrogen atmosphere. The mixture was heated to 80 °C in an oil bath, during which the suspension turned reddish-brown, and the temperature of the bath rose to 92 °C. After 30 min, the temperature of the oil bath was lowered to 80 °C and maintained for 2 h. The mixture was then allowed to cool to 23 °C and stirred for about 20 h and then was poured into 1N HCl solution (150 mL). After stirring the mixture for 30 min, the precipitate was filtered, washed extensively with water and diethyl ether, and dried to afford **3a** as a light-gray solid (2.56 g, 89%). ¹H NMR (500 MHz, DMSO-*d*₆) δ 12.99 (s, 1H), 10.72 (s, 1H), 7.55 (s, 1H), 7.50 (d, *J* = 7.9 Hz, 1H), 7.42 (d, *J* = 7.9 Hz, 1H), 3.31 (s, 2H). LRMS (ESI-ve): calculated for C₉H₆NO₃S, [M – H] = 208.01; observed, [M – H] = 207.95. (*Z*)-2-(2-Fluorobenzylidene)-3-oxo-3,4-dihydro-2H-benzo[b][1,4]thiazine-6-carboxylic Acid (**4a**) **3a** (1.2 g, 5.7 mmol), was suspended in acetic anhydride (20 mL) in a 40 mL vial. Triethylamine (2.39 mL, 17.2 mmol) and 2-fluorobenzaldehyde (1.21 mL, 11.5 mmol) were added, and the mixture was heated at 145 °C for 15 h. The reaction mixture was cooled to 23 °C, poured into 100 mL of diethyl ether, and cooled at 4 °C for 20 min. The precipitate was collected by filtration, washed with ether (25 mL), and dried to afford **4a** as a yellowish-brown solid (1.28 g, 71%). ¹H NMR (500 MHz, DMSO-*d*₆) δ 11.30 (s, 1H), 7.86 (s, 1H), 7.79 (t, 1H), 7.69 (d, *J* = 1.7 Hz, 1H), 7.55 (dd, *J* = 8.3, 1.7 Hz, 1H), 7.53–7.48 (m, 1H), 7.43 (d, *J* = 8.2 Hz, 1H), 7.40–7.33 (m, 2H). LRMS (ESI-ve): calculated for C₁₆H₁₀FNO₃S, [M – H] = 314.03; observed, [M – H] = 314.0.

(*R,Z*)-N-((1-Ethylpyrrolidin-2-yl)methyl)-2-(2-fluorobenzylidene)-3-oxo-3,4-dihydro-2H-benzo[b][1,4]thiazine-6-carboxamide (**11**). **4a** (300 mg, 0.95 mmol), HOBT (193 mg, 1.43 mmol), and EDCI-HCl

(274 mg, 1.43 mmol) were combined in an 8 mL vial. Dry dichloromethane (4 mL) and triethylamine (0.4 mL, 2.85 mmol) were added, and the mixture was stirred at 23 °C for 5 min. (*R*)-(1-Ethylpyrrolidin-2-yl)methanamine (0.2 mL, 1.43 mmol) was added, and within a few minutes the solution became homogeneous and was allowed to stir for about 15 h. The reaction mixture was then diluted with 20% methanol/dichloromethane (5 mL) and extracted with water (4 mL, 3×). The organic layer was dried over anhydrous sodium sulfate and evaporated to afford a brown residue. The residue was purified by RP-HPLC on a SunFire preparative C18 column (5 μm; 19 mm × 50 mm) using a stepwise gradient {10% [(MeCN + 0.1% TFA) in (water + 0.1% TFA)] for 1 min, 30% for 1 min, 50% for 4 min, 70% for 1.5 min, and 98% for 1.5 min}. The fractions containing the expected molecular weight were collected and freeze-dried to afford a formate salt of the product as a pale-yellow solid. The solid was dissolved in dichloromethane and extracted with 25% K₂CO₃ solution (3×). The organic layer was dried over anhydrous sodium sulfate and evaporated to afford **11** as a yellowish–brown solid (0.13 g, 32%); mp = 194–197 °C; [α]_D = (+)-12.9 (*c* = 0.001, MeOH, 23 °C). ¹H NMR (500 MHz, acetic acid-*d*₄) δ 8.05 (s, 1H), 7.83 (t, *J* = 7.3 Hz, 1H), 7.60 (dd, *J* = 8.3, 1.7 Hz, 1H), 7.52 (d, *J* = 1.6 Hz, 1H), 7.44 (dd, *J* = 13.3, 6.3 Hz, 1H), 7.36 (d, *J* = 8.3 Hz, 1H), 7.31 (t, *J* = 7.5 Hz, 1H), 7.20 (t, *J* = 7.5 Hz, 1H), 3.98–3.76 (m, 4H), 3.54–3.41 (m, 1H), 3.23–3.08 (m, 2H), 2.37–2.22 (m, 1H), 2.12–2.05 (m, 3H), 1.33 (t, *J* = 7.5 Hz, 3H). For ¹H NMR in methanol-*d*₄, see Supporting Information. LRMS (ESI+ve): calculated for C₂₃H₂₄FN₃O₂S, [M + H] = 426.17; observed, [M + H] = 426.26. HRMS (ESI+ve): calculated for C₂₃H₂₄FN₃O₂S, [M + H] = 426.1646; observed, [M + H] = 426.1631.

Activity against *P. falciparum* in Culture. The chloroquine-sensitive *P. falciparum* 3D7 and the resistant Dd2 strains were cultured as described elsewhere.³⁸ Effects of PfGluPho inhibitors on *Plasmodium* parasites were tested using isotopic drug sensitivity assays,^{39,40} which are based on the incorporation of radioactive ³H-hypoxanthine. Hypoxanthine is taken up by *Plasmodium* parasites because it is needed for nucleic acid synthesis. In brief, *P. falciparum*-infected RBCs were seeded in 96-well plates (Nunc) at a parasitemia of 0.25% (>70% ring forms) and 1.25% hematocrit in hypoxanthine-free medium. Varying concentrations of the test compounds and the control chloroquine (Sigma) were added to the wells. The parasites were incubated for 48 h, after which 0.5 μCi ³H-hypoxanthine was added for a further 24 h. The cells of each well were harvested on a glass fiber filter (Perkin-Elmer), washed, and dried. Finally, the radioactivity of each condition was detected, which is supposed to be proportional to the parasites' growth. IC₅₀ values were calculated using nonlinear regression of the GraphPad Prism software.

MOI Studies. PfGluPho inhibitors were mechanistically characterized as previously described.³⁴ In brief, varying G6P or NADP⁺ concentrations were prepared in a substrate solution (final assay concentration (FAC) 3.3 mM MgCl₂, 1 mM TCEP, 0.05 M Tris; for G6P titration, 5 μM NADP⁺; for NADP⁺ titration, 25 μM G6P) and transferred to 384-well plate. Varying compound concentrations (starting at around 8× IC₅₀) titrated in DMSO were added to the wells using the Echo Liquid Handler. Addition of an enzyme mix (FAC 0.2 μg/mL PfGluPho, 0.005% Tween 20) started the reaction. Fluorescence of NADPH production was monitored over 10 min at ex340/em460 with a SpectraMax M5 (Molecular Devices) multiwell plate reader, and the initial slope was determined with the SoftMax Pro 5.2 software (Molecular Devices). On the basis of the data, Lineweaver–Burk plots were created,⁴¹ and *K*_m and *V*_{max} values were calculated with the GraphPad Prism software. Additionally, α from the following rate equation was calculated using SigmaPlot (Systat Software) (eq 1; *v* = velocity, *S* = substrate, *I* = inhibitor).

$$v = \frac{V_{\max}^{\text{app}}[S]}{K_m^{\text{app}} + [S]}$$

$$\text{where } V_{\max}^{\text{app}} = \frac{V_{\max}}{(1 + [I]/\alpha K_i)} \text{ and } K_m^{\text{app}} = K_m \frac{(1 + [I]/K_i)}{(1 + [I]/\alpha K_i)} \quad (1)$$

If Lineweaver–Burk plots intersected at the *y* axis, *K*_m^{app} increased, and *V*_{max}^{app} was constant with increasing inhibitor concentrations, α = ∞, then compounds were assigned to inhibit competitively. Lineweaver–Burk plots intersecting at the *x* axis, constant *K*_m^{app} and decreasing *V*_{max}^{app} values with increasing inhibitor concentrations, and α = 1 indicated noncompetitive inhibition. Parallel lines in Lineweaver–Burk plots, decreasing *K*_m^{app} and *V*_{max}^{app} values with increasing inhibitor concentration, and α < 1 was characteristic for uncompetitive inhibition.⁴² Were parameters found to be between those for competitive and noncompetitive inhibitors, compounds were assigned to follow mixed-type inhibition.

Protocol for Chemical Stability (Reactivity/GSH Adduct Formation). Protocol: 10 μL of compound (1 mM stock in DMSO) was added to 985 μL of PBS buffer (1×, pH = 7.4) in a capped glass vial. Then 5 μL of GSH solution (10 mM stock in PBS) was added to the solution, and the mixture was gently mixed on a Grant-Bio PS-M3D platform shaker at 23 °C. Then 20 mL aliquots were analyzed at 0, 0.5, 1, 2, 4, 6, 18, and 25 h on a Waters HPLC-MS system using a SunFire analytical C18 column (5 μm; 4.6 mm × 50 mm) using a stepwise gradient [11 {10% [(MeCN + 0.1% TFA) in (water + 0.1% TFA)] for 1 min, 30% for 1 min, 50% for 4 min, 70% for 1.5 min, and 98% for 1.5 min}; ethacrynic acid {10% [(MeCN + 0.1% TFA) in (water + 0.1% TFA)] for 1 min, 30% for 1 min, 50% for 4 min, 70% for 1.5 min, and 98% for 1.5 min}. The percentage remaining for each compound relative to the starting amount of compound at 0 h was calculated from the area under the curve (AUC) at different time points and plotted.

■ ASSOCIATED CONTENT

📄 Supporting Information

Detailed experimental procedures for the synthesis of **1b**, **1c**, **2b**, **2c**, **3b–3d**, **4b–4j**, **5a–5j**, **10**, **12–15**, **17**, **22**, **29**, **33**, **34**, and **39–42** as well as NMR spectra of **2a**, **3a**, **3d**, **4a**, **5a–5j**, **10**, **11** (acetic acid-*d*₄), **11** (methanol-*d*₄), **12–15**, **17**, **22**, **29**, **33**, **34**, and **39–42**. This material is available free of charge via the Internet at <http://pubs.acs.org>.

■ AUTHOR INFORMATION

✉ Corresponding Author

*For K.B.: phone, +49-641-9939121; fax, +49-641-9939129; E-mail, katja.becker@uni-giessen.de. For A.B.P.: phone, 01-858-695-5320; E-mail, apinkerton@sanfordburnham.org. For L.B.: phone, 01-619-543-7545; fax, 01-619-543-7537; E-mail, lbode@ucsd.edu.

✍ Author Contributions

[†]These authors contributed equally to this work

📝 Notes

The authors declare no competing financial interest.

■ ACKNOWLEDGMENTS

We thank Michaela Stumpf, Beate Hecker, and Elisabeth Fischer for their excellent technical assistance. The study was supported by the NIH (1R21AI082434-01) to L.B., the Deutsche Forschungsgemeinschaft (BE 1540/18-1) to K.B., and an NIH Molecular Libraries grant (U54 HG005033-03) to the Conrad Prebys Center for Chemical Genomics at the Sanford Burnham Medical Research Institute, one of the comprehensive centers of the NIH Molecular Libraries Probe Production Centers Network (MLPCN).

■ ABBREVIATIONS USED

ADME/T, absorption distribution metabolism excretion toxicity; AUC, area under the curve; BBB, blood-brain barrier; CBIS, Chemical and Biological Information Systems; EDCl, 1-ethyl-3-(3-dimethylaminopropyl) carbodiimide; ESI, electron spray ionization; ex/em, excitation/emission; FAC, final assay

concentration; G6P, glucose-6-phosphate; G6PD, glucose-6-phosphate dehydrogenase; hG6PD, human glucose-6-phosphate dehydrogenase; HRMS, high resolution mass spectrometry; HTS, high-throughput screening; IRBC, infected red blood cells; MLSMR, Molecular Libraries Small Molecule Repository; MOI, mechanism of inhibition; PAMPA, parallel artificial membrane permeability assay; PfG6PD, *Plasmodium falciparum* glucose-6-phosphate dehydrogenase; PfGluPho, *Plasmodium falciparum* glucose-6-phosphate dehydrogenase 6-phosphogluconolactonase; PPP, pentose phosphate pathway; RNAi, RNA interference; SAR, structure–activity relationship; TOF, time-of-flight

REFERENCES

- (1) Murray, C. J. L.; Rosenfeld, L. C.; Lim, S. S.; Andrews, K. G.; Foreman, K. J.; Haring, D.; Fullman, N.; Naghavi, M.; Lozano, R.; Lopez, A. D. Global malaria mortality between 1980 and 2010: a systematic analysis. *Lancet* **2012**, *379*, 413–431.
- (2) *World Malaria Report 2008*; World Health Organization: Geneva, 2008; http://whqlibdoc.who.int/publications/2008/9789241563697_eng.pdf.
- (3) Baron, J. M.; Higgins, J. M.; Dzik, W. H. A revised timeline for the origin of *Plasmodium falciparum* as a human pathogen. *J. Mol. Evol.* **2011**, *73*, 297–304.
- (4) Tanabe, K.; Mita, T.; Jombart, T.; Eriksson, A.; Horibe, S.; Palacpac, N.; Ranford-Cartwright, L.; Sawai, H.; Sakihama, N.; Ohmae, H.; Nakamura, M.; Ferreira, M. U.; Escalante, A. A.; Prugnolle, F.; Bjorkman, A.; Farnert, A.; Kaneko, A.; Horii, T.; Manica, A.; Kishino, H.; Balloux, F. *Plasmodium falciparum* accompanied the human expansion out of Africa. *Curr. Biol.* **2010**, *20*, 1283–1289.
- (5) Rodrigues, T.; Moreira, R.; Lopes, F. New hope in the fight against malaria? *Future Med. Chem.* **2011**, *3*, 1–3.
- (6) Hill, A. V. Vaccines against malaria. *Philos. Trans. R. Soc., B* **2011**, *366*, 2806–2814.
- (7) Murambiwa, P.; Masola, B.; Govender, T.; Mukaratirwa, S.; Musabayane, C. T. Anti-malarial drug formulations and novel delivery systems: a review. *Acta Trop.* **2011**, *118*, 71–79.
- (8) Bousejra-El Garah, F.; Wong, M. H.; Amewu, R. K.; Muangnoicharoen, S.; Maggs, J. L.; Stigliani, J. L.; Park, B. K.; Chadwick, J.; Ward, S. A.; O'Neill, P. M. Comparison of the reactivity of antimalarial 1,2,4,5-tetraoxanes with 1,2,4-trioxolanes in the presence of ferrous iron salts, heme, and ferrous iron salts/phosphatidylcholine. *J. Med. Chem.* **2011**, *54*, 6443–6455.
- (9) Schlitzer, M. Antimalarial drugs—What is in use and what is in the pipeline. *Arch. Pharm.* **2008**, *341*, 149–163.
- (10) Murambiwa, P.; Masola, B.; Govender, T.; Mukaratirwa, S.; Musabayane, C. T. Anti-malarial drug formulations and novel delivery systems: A review. *Acta Trop.* **2011**, *118*, 71–79.
- (11) Trape, J. F. The public health impact of chloroquine resistance in Africa. *Am. J. Trop. Med. Hyg.* **2001**, *64*, 12–17.
- (12) Marks, F.; von Kalckreuth, V.; Kobbe, R.; Adjei, S.; Adjei, O.; Horstmann, R. D.; Meyer, C. G.; May, J. Parasitological rebound effect and emergence of pyrimethamine resistance in *Plasmodium falciparum* after single-dose sulfadoxine-pyrimethamine. *J. Infect. Dis.* **2005**, *192*, 1962–1965.
- (13) Egan, T. J.; Kaschula, C. H. Strategies to reverse drug resistance in malaria. *Curr. Opin. Infect. Dis.* **2007**, *20*, 598–604.
- (14) Gottschall, J. L.; Elliot, W.; Lianos, E.; McFarland, J. G.; Wolfmeyer, K.; Aster, R. H. Quinine-induced immune thrombocytopenia associated with hemolytic uremic syndrome: a new clinical entity. *Blood* **1991**, *77*, 306–310.
- (15) Veinot, J. P.; Mai, K. T.; Zarychanski, R. Chloroquine related cardiac toxicity. *J. Rheumatol.* **1998**, *25*, 1221–1225.
- (16) *Guidelines for the Treatment of Malaria*; World Health Organization: Geneva, 2010; http://whqlibdoc.who.int/publications/2010/9789241547925_eng.pdf.
- (17) Dondorp, A. M.; Nosten, F.; Yi, P.; Das, D.; Phyo, A. P.; Tarning, J.; Lwin, K. M.; Ariey, F.; Hanpithakpong, W.; Lee, S. J.; Ringwald, P.; Silamut, K.; Imwong, M.; Chotivanich, K.; Lim, P.; Herdman, T.; An, S. S.; Yeung, S.; Singhasivanon, P.; Day, N. P.; Lindegardh, N.; Socheat, D.; White, N. J. Artemisinin resistance in *Plasmodium falciparum* malaria. *N. Engl. J. Med.* **2009**, *361*, 455–467.
- (18) Noedl, H.; Se, Y.; Sriwichai, S.; Schaecher, K.; Teja-Isavadharm, P.; Smith, B.; Rutvisuttinunt, W.; Bethell, D.; Surasri, S.; Fukuda, M. M.; Socheat, D.; Chan Thap, L. Artemisinin resistance in Cambodia: a clinical trial designed to address an emerging problem in Southeast Asia. *Clin. Infect. Dis.* **2010**, *51*, e82–e89.
- (19) Carrara, V. I.; Zwang, J.; Ashley, E. A.; Price, R. N.; Stepniewska, K.; Barends, M.; Brockman, A.; Anderson, T.; McGready, R.; Phaiphun, L.; Proux, S.; van Vugt, M.; Hutagalung, R.; Lwin, K. M.; Phyo, A. P.; Preechapornkul, P.; Imwong, M.; Pukrittayakamee, S.; Singhasivanon, P.; White, N. J.; Nosten, F. Changes in the treatment responses to artesunate-mefloquine on the northwestern border of Thailand during 13 years of continuous deployment. *PLoS One* **2009**, *4*, e4551.
- (20) Jortzik, E.; Mailu, B. M.; Preuss, J.; Fischer, M.; Bode, L.; Rahlfs, S.; Becker, K. Glucose-6-phosphate dehydrogenase-6-phosphogluconolactonase: a unique bifunctional enzyme from *Plasmodium falciparum*. *Biochem. J.* **2011**, *436*, 641–650.
- (21) Nkhoma, E. T.; Poole, C.; Vannappagari, V.; Hall, S. A.; Beutler, E. The global prevalence of glucose-6-phosphate dehydrogenase deficiency: a systematic review and meta-analysis. *Blood Cells Mol. Dis.* **2009**, *42*, 267–278.
- (22) Luzzatto, L. Glucose 6-phosphate dehydrogenase deficiency: from genotype to phenotype. *Haematologica* **2006**, *91*, 1303–1306.
- (23) Cappadoro, M.; Giribaldi, G.; O'Brien, E.; Turrini, F.; Mannu, F.; Ulliers, D.; Simula, G.; Luzzatto, L.; Arese, P. Early phagocytosis of glucose-6-phosphate dehydrogenase (G6PD)-deficient erythrocytes parasitized by *Plasmodium falciparum* may explain malaria protection in G6PD deficiency. *Blood* **1998**, *92*, 2527–2534.
- (24) Ruwende, C.; Khoo, S. C.; Snow, R. W.; Yates, S. N.; Kwiatkowski, D.; Gupta, S.; Warn, P.; Allsopp, C. E.; Gilbert, S. C.; Peschu, N.; et al. Natural selection of hemi- and heterozygotes for G6PD deficiency in Africa by resistance to severe malaria. *Nature* **1995**, *376*, 246–249.
- (25) Atamna, H.; Pascarmona, G.; Ginsburg, H. Hexose-monophosphate shunt activity in intact *Plasmodium falciparum*-infected erythrocytes and in free parasites. *Mol. Biochem. Parasitol.* **1994**, *67*, 79–89.
- (26) Preuss, J.; Jortzik, E.; Becker, K. Glucose-6-phosphate metabolism in *Plasmodium falciparum*. *IUBMB Life* **2012**, *64*, 603–611.
- (27) Becker, K.; Koncarevic, S.; Hunt, N. H. Oxidative stress and antioxidant defense in malarial parasites. In *Molecular Approaches to Malaria*; Sherman, I. W., Ed.; American Society of Microbiology Press: Washington DC, 2005; pp 365–383.
- (28) Crooke, A.; Diez, A.; Mason, P. J.; Bautista, J. M. Transient silencing of *Plasmodium falciparum* bifunctional glucose-6-phosphate dehydrogenase-6-phosphogluconolactonase. *FEBS J.* **2006**, *273*, 1537–1546.
- (29) Baum, J.; Papenfuss, A. T.; Mair, G. R.; Janse, C. J.; Vlachou, D.; Waters, A. P.; Cowman, A. F.; Crabb, B. S.; de Koning-Ward, T. F. Molecular genetics and comparative genomics reveal RNAi is not functional in malaria parasites. *Nucleic Acids Res.* **2009**, *37*, 3788–3798.
- (30) Lopez-Barragan, M. J.; Lemieux, J.; Quinones, M.; Williamson, K. C.; Molina-Cruz, A.; Cui, K.; Barillas-Mury, C.; Zhao, K.; Su, X. Z. Directional gene expression and antisense transcripts in sexual and asexual stages of *Plasmodium falciparum*. *BMC Genomics* **2011**, *12*, 587.
- (31) Clarke, J. L.; Scopes, D. A.; Sodeinde, O.; Mason, P. J. Glucose-6-phosphate dehydrogenase-6-phosphogluconolactonase. A novel bifunctional enzyme in malaria parasites. *Eur. J. Biochem.* **2001**, *268*, 2013–2019.
- (32) Clarke, J. L.; Sodeinde, O.; Mason, P. J. A unique insertion in *Plasmodium berghei* glucose-6-phosphate dehydrogenase-6-phosphogluconolactonase: evolutionary and functional studies. *Mol. Biochem. Parasitol.* **2003**, *127*, 1–8.

(33) ML276 has been declared a probe via the Molecular Libraries Probe Production Centers Network (MLPCN) and is available through the network, see: <http://mli.nih.gov/mli/>.

(34) Preuss, J.; Hedrick, M.; Sergienko, E.; Pinkerton, A.; Mangravita-Novo, A.; Smith, L.; Marx, C.; Fischer, E.; Jortzik, E.; Rahlfs, S.; Becker, K.; Bode, L. High-throughput screening for small-molecule inhibitors of *Plasmodium falciparum* glucose-6-phosphate dehydrogenase 6-phosphogluconolactonase. *J. Biomol. Screening* **2012**, *17*, 738–751.

(35) Trifilenkov, A. S.; Kobak, V. V.; Salina, M. A.; Kusovkova, J. A.; Ilyin, A. P.; Khvat, A. V.; Tkachenko, S. E.; Ivachtchenko, A. V. Liquid-phase parallel synthesis of combinatorial libraries of substituted 6-carbamoyl-3,4-dihydro-2H-benzo[1,4]thiazines. *J. Comb. Chem.* **2006**, *8*, 469–479.

(36) Worley, J. W.; Ratts, K. W.; Cammack, K. L. 2-Dialkylphosphonyl- and 2-Alkylidene-3,4-dihydro-3-oxo-2H-1,4-benzothiazines. *J. Org. Chem.* **1975**, *40*, 1731–1734.

(37) Ploemen, J. H.; Van Schanke, A.; Van Ommen, B.; Van Bladeren, P. J. Reversible conjugation of ethacrynic acid with glutathione and human glutathione S-transferase P1–1. *Cancer Res.* **1994**, *54*, 915–919.

(38) Koncarevic, S.; Rohrbach, P.; Deponte, M.; Krohne, G.; Prieto, J. H.; Yates, J., III; Rahlfs, S.; Becker, K. The malarial parasite *Plasmodium falciparum* imports the human protein peroxiredoxin 2 for peroxide detoxification. *Proc. Natl. Acad. Sci. U.S.A.* **2009**, *106*, 13323–13328.

(39) Desjardins, R. E.; Canfield, C. J.; Haynes, J. D.; Chulay, J. D. Quantitative assessment of antimalarial activity in vitro by a semiautomated microdilution technique. *Antimicrob. Agents Chemother.* **1979**, *16*, 710–718.

(40) Fivelman, Q. L.; Adagu, I. S.; Warhurst, D. C. Modified fixed-ratio isobologram method for studying in vitro interactions between atovaquone and proguanil or dihydroartemisinin against drug-resistant strains of *Plasmodium falciparum*. *Antimicrob. Agents Chemother.* **2004**, *48*, 4097–4102.

(41) Cornish-Bowden, A.: Introduction to enzyme kinetics. In *Fundamentals of Enzyme Kinetics*, 3rd ed.; Cornish-Bowden, A., Ed.; Portland Press: London, 2004.

(42) Cornish-Bowden, A.: Reversible inhibition and activation. In *Fundamentals of Enzyme Kinetics*, 3rd ed.; Cornish-Bowden, A., Ed.; Portland Press: London, 2004.